

Impurity effects on phase and microstructure stabilities of reactively-sintered porous MgTi₂O₅

Xinzhu MIAO^a, Yoshikazu SUZUKI^{a,b*}

^a Graduate School of Pure and Applied Sciences, University of Tsukuba, 1-1-1 Tennodai, Tsukuba, Ibaraki 305-8573, Japan

^b Faculty of Pure and Applied Sciences, University of Tsukuba, 1-1-1 Tennodai, Tsukuba, Ibaraki 305-8573, Japan

Abstract:

Since the thermal-expansion anisotropy of pseudobrookite-type MgTi₂O₅ is not as prominent as isomorphous Al₂TiO₅, MgTi₂O₅ is thermally more stable than Al₂TiO₅. To realize the future structural applications of porous MgTi₂O₅, influence of impurities on the phase and microstructure stabilities should be studied. Here, impurity effects on phase and microstructure stabilities of reactively-sintered porous MgTi₂O₅ have been studied. As model impurities, Li₂CO₃ and amorphous SiO₂ have been selected. Li₂CO₃ or SiO₂ powder (0.1-4.0 wt.%) was added to MgCO₃ (basic) and TiO₂ anatase powders with a molar ratio of 1:2. Uniaxially-pressed mixed powders were sintered at 1100°C in air for 2 h to obtain porous MgTi₂O₅ bars. Appropriate Li₂CO₃ and SiO₂ doping (~0.5 wt.%) promoted uniform grain growth. However, with the excess amount of the impurities (> 2 wt.%), the coefficient of thermal expansion of Li₂CO₃- and SiO₂-doped MgTi₂O₅ ceramics decreased obviously above 900°C and 950°C due to the secondary sintering. To keep the fine-grained porous microstructure of Li₂CO₃- and SiO₂-doped samples with preventing the secondary sintering, impurity levels should be preferably limited less than ~1.0 wt.%.

Key-words:

A. Powders: solid state reaction; A. Sintering; B. Impurities; C: Thermal expansion

1. Introduction

Diesel particulate filters (DPFs) are widely used for collecting particulate matter (PM) in the diesel exhaust gas [1-4]. Since it is necessary to regenerate the filter function by burning out the trapped PM in the DPF, high thermal-shock resistance is indispensable, which is realized by low thermal expansion as well as high mechanical strength, high thermal conductivity and low Young's modulus [1]. Cordierite (2MgO·2Al₂O₃·5SiO₂) and silicon carbide (SiC) have been

* Corresponding author (suzuki@ims.tsukuba.ac.jp)
Division of Materials Science, Faculty of Pure and Applied Sciences, University of Tsukuba, Ibaraki 305-8573, Japan

widely used as wall-flow type DPF materials. Cordierite, a light-weight silicate-based compound, exhibits excellent low thermal expansion, so it is possible to integrally mold a large-sized honeycomb. It is superior in terms of the production cost due to low-cost natural resources and a reactive sintering process in air. The heat resistance of cordierite, however, is somewhat insufficient as compared with that of SiC. As for the SiC DPF, despite its excellent heat resistance and mechanical strength, its thermal expansion is much larger than that of cordierite, and hence additional steps of forming and bonding small segments with typical cross-sections of $\sim 3 \text{ cm} \times 3 \text{ cm}$ are required [4]. That is somewhat disadvantageous in terms of the production cost.

Both cordierite (the first generation) and SiC (the second generation) DPFs have excellent track records in the market, but still, nonsilicate-oxide-based DPFs (the third generation) enabling both low-cost and excellent heat resistance have been developed and are recently put into practical use [5,6]. Aluminum titanate (Al_2TiO_5 , AT) having pseudobrookite-type structure is promising as a third-generation DPF material. The pseudobrookite-type crystal structure exhibits highly anisotropic thermal expansion [7], which induces the formation of intergranular and intragranular microcracks. These microcracks relax the thermal stress of particles, and hence, the pseudobrookite-type ceramics generally have low coefficient of bulk thermal expansion. A possible weak point of AT, however, is its instability at middle-range temperatures; Al_2TiO_5 is metastable below $1200 \text{ }^\circ\text{C}$ due to the large distortion of MeO_6 -octahedra, and thus undoped- Al_2TiO_5 tends to decompose into Al_2O_3 and TiO_2 . At the present time, US Corning [5] and Sumitomo Chemical Co. [8] have succeeded in the commercialization of AT-based DPFs with some oxide additives for improving the middle-range temperature stability. The AT-based DPF can be integrally molded and sintered in an air atmosphere, as with cordierite. Due to its high heat resistance, AT-based DPF shows high performance (secondarily to SiC DPF) at relatively low cost.

Since the thermal-expansion anisotropy of another pseudobrookite-type compound, MgTi_2O_5 (MT_2), is not as prominent as Al_2TiO_5 , MgTi_2O_5 is thermally more stable than Al_2TiO_5 [9-16]. Recently, Suzuki et al. [17-24] have focused on MgTi_2O_5 as potential materials for third generation DPFs, water purification filters and light-weight structural components. To realize the future applications of MT_2 -based components, influence of impurities (either in starting materials or during processing) on phase and microstructure stabilities of porous MgTi_2O_5 should be studied. Here, impurity effects on phase and microstructure stabilities of reactively-sintered porous MgTi_2O_5 have been studied. As model impurities, Li_2CO_3 (melting point: $723 \text{ }^\circ\text{C}$, decomposition temperature: $\sim 1300 \text{ }^\circ\text{C}$) and amorphous SiO_2 (i.e. a typical impurity from natural resources) have been selected.

2. Experimental procedures

The raw materials used to prepare porous MgTi_2O_5 ceramics were MgCO_3 (basic) powder (99.9% purity, $\text{Mg}_5(\text{CO}_3)_4(\text{OH})_2 \cdot 4\text{H}_2\text{O}$, hydromagnesite) and TiO_2 anatase powder (99.9%, Kojundo Chemical Laboratory Co. Ltd.) with a molar ratio of 1:2. As simulated impurities, Li_2CO_3 powder (99%, Wako Pure Chemical) or SiO_2 powder (99.9%, amorphous, Wako Pure Chemical) with a different amount (0.1 wt.%, 0.5 wt.%, 1.0 wt.%, 2.0 wt.%, or 4.0 wt.%) was added to prepare the mixed powders. The powders were wet-ball milled with ZrO_2 balls in ethanol for 24 h. The mixed slurries were vacuum dried and placed into an oven at 80°C overnight. The dried powders were then sieved through a 150-mesh screen. The mixed powders were then uniaxially pressed into rectangular bars of $5 \times 6 \times 50$ mm at the pressure of 18 MPa for 1 min. After pressing, the samples were sintered at 1100°C in air for 2 h to obtain porous MgTi_2O_5 bars. Phase analysis was performed with X-ray diffraction (XRD, $\text{Cu-K}\alpha$, 40 kV and 40 mA, Multiflex, Rigaku, Japan). The density was determined by the dimensions and mass. The microstructure of porous MgTi_2O_5 ceramics was observed by scanning electron microscopy (SEM, JSM-5600LV, JEOL, Japan). The pore-size distributions and the pore volumes were determined by the mercury porosimetry (AutoPore IV 9520, Micromeritics).

Coefficient of thermal expansion (CTE) of the porous MgTi_2O_5 bars (~15-18 mm) was determined by the thermal mechanical analysis (TMA, Thermal plus EVO, Rigaku, Japan). In order to evaluate the fracture strength, sintered rectangular bars were machined into the test specimens. The tensile face and corners of each specimen were polished and chamfered by waterproof abrasive paper. Fracture strength was measured by the three-point bending test with a span of 30 mm and a crosshead speed of 0.5mm/min by using a universal testing machine (Autograph AG-20kN, Shimadzu Co. Ltd., Japan). Three specimens were used for each measurement.

3. Results and discussion

3.1 Phase analysis

Figure 1 shows XRD patterns of porous MgTi_2O_5 with (a) Li_2CO_3 and (b) SiO_2 impurities. As can be seen in Fig. 1 (a), without any impurity, MgO and TiO_2 reacted to form single-phase MgTi_2O_5 by the reactive sintering at 1100°C . However, with Li_2CO_3 impurity, a small amount of MgTiO_3 remained as an intermediate product. MgTiO_3 peaks became stronger with increasing the amount of Li_2CO_3 , similarly to the previous report with LiF doping [21]. To form the final MgTi_2O_5 phase, intermediate MgTiO_3 particles should further react with TiO_2 particles. In the interior of the porous body, however, some *isolated* MgTiO_3 particles on the anisotropically-grown MgTi_2O_5 particles could not further react with TiO_2 . This hypothesis is well-supported by the mercury porosimetry in the latter part, which clearly demonstrated the

enlargement of the pore size by the addition of Li_2CO_3 . Note that the effective ionic radii of 6-coordinate Li^+ and Mg^{2+} are 0.76 Å and 0.720 Å [25], some Li^+ may dissolve in MgTi_2O_5 and MgTiO_3 phases, without apparent changes of lattice parameters. Excess TiO_2 then probably compensated the formation of MgTi_2O_5 (ss) and MgTiO_3 (ss).

With SiO_2 impurity (Fig. 1 (b)), TiO_2 rutile peaks were confirmed for the samples with ≥ 0.5 wt.% SiO_2 , and Mg_2SiO_4 (forsterite) peaks were confirmed for those with ≥ 2.0 wt.% SiO_2 . TiO_2 rutile was formed by the phase transformation of unreacted TiO_2 anatase, and Mg_2SiO_4 was yielded as a byproduct. Contrary to the Li_2CO_3 case, decrease of the pore size by the addition of SiO_2 was observed (via the mercury porosimetry as shown in the latter part), which is in good agreement with the no intermediate MgTiO_3 in the final product.

3.2 Bulk density and apparent porosity

Figure 2 shows the bulk density of porous MgTi_2O_5 with (a) Li_2CO_3 and (b) SiO_2 impurities. Relative density values (insert) were nominally calculated from the theoretical density of MgTi_2O_5 , 3.644 g/cm³, without taking into account second phases. Volume shrinkage with Li_2CO_3 impurity is also demonstrated (insert). It can be obviously seen from Fig. 2 (a) that the bulk density linearly increased with increasing the amount of Li_2CO_3 . The result indicates that Li_2CO_3 -doping may be an effective way to control the bulk density of porous MgTi_2O_5 . With SiO_2 impurity (Fig. 2 (b)), bulk density increased (up to ~0.5 wt.%), and then decreased (with the amount of SiO_2). The increase can be explained by the formation of glassy phase SiO_2 , and the decrease may be explained by the formation of second phases (as well as the intrinsic light-weight nature of SiO_2).

3.3 Microstructure

Figure 3 shows the microstructure of (a) non-doped porous MgTi_2O_5 , (b)-(f) porous MgTi_2O_5 with Li_2CO_3 and (g)-(k) porous MgTi_2O_5 with SiO_2 . The non-doped porous MgTi_2O_5 sample presented a microstructure with small particle size and relatively narrow pore-size distribution (Fig. 3(a)). For the Li_2CO_3 -doped samples, the grain size increased with increasing the amount of Li_2CO_3 . Liquid phase formation during the reactive sintering caused the grain growth due to the low melting point of Li_2CO_3 (~723°C, or even less due to the eutectic formation). For example, the sample with 2.0 wt.% Li_2CO_3 presented a uniform microstructure with the typical grain size of ~1-2 μm (Fig. 3(e)). Excess Li_2CO_3 addition promoted inhomogeneous localized sintering and may form some closed pores (Fig. 3(f)), thereby reducing porosity of MgTi_2O_5 ceramics.

As can be seen in Fig. 3 (g), the sample with 0.1 wt.% SiO_2 contained relatively large flaw probably due to inhomogeneous dispersion of SiO_2 . The sample with 0.5 wt.% SiO_2

presented a uniform 3-D network microstructure (Fig. 3(h)), similarly to the reported porous MgTi_2O_5 with 0.5 wt.% LiF additive [18]. Excess SiO_2 addition (≥ 1.0 wt.% SiO_2) promoted inhomogeneous localized sintering, similarly to Fig. 3(f), but suppressed grain growth. From the SEM observation for the 1100°C-sintered samples, excess Li_2CO_3 (with low melting point) accelerated the grain growth by liquid phase formation, whereas excess amorphous SiO_2 suppressed the grain growth and formed inhomogeneous microstructure.

Figure 4 and **Table 2** show the pore-size distributions and the pore volumes measured by the mercury porosimetry. As can be seen in Fig. 4 and Table 2, although both Li_2CO_3 and SiO_2 doping decreased the pore volume, the Li_2CO_3 doping increased the pore size, whereas the SiO_2 doping decreased the pore size. These results are in good agreement with the SEM observation.

3.3 The coefficient of thermal expansion

Figure 5 presents the thermal expansion curves and the thermal expansion coefficients of MgTi_2O_5 with Li_2CO_3 and SiO_2 impurities. For the samples with Li_2CO_3 (Figs. 5 (a) and (b)), there were little or no significant difference on thermal expansion between non-doped and ≤ 2 wt.% Li_2CO_3 -doped MgTi_2O_5 samples up to 900°C. The 4 wt.% Li_2CO_3 -doped MgTi_2O_5 showed higher thermal expansion, probably due to the increasing of intermediate MgTiO_3 phases, as shown in Fig. 1(a). Decrease of the thermal expansion above 900°C for all the Li_2CO_3 -doped MgTi_2O_5 samples can be attributed to the further densification (secondary sintering) during the TMA measurement. For the samples with SiO_2 additives (Figs. 5 (c) and (d)), the thermal expansion and CTE curves were almost the same for all compositions. The bulk thermal expansion slightly decreased above 950°C, which can be also attributed to the secondary sintering. Hence, the structural applications of fine-grained porous MgTi_2O_5 ceramics with Li_2CO_3 -doping are preferably at less than 900°C, and those with SiO_2 -doping are preferably less than 950°C.

3.4 Mechanical properties

Figure 6 shows the 3-point bending fracture strength of porous MgTi_2O_5 with different impurities. Fracture strength of the sample with Li_2CO_3 impurity was almost constant up to 2.0 wt.% addition, but their error bars became larger for the 1.0 and 2.0 samples. Fracture strength of the sample with 4.0 wt.% Li_2CO_3 increased to 33.2 MPa due to the progress of densification (see Figs. 2(a) and 3 (f)). Fracture strength of the sample with 0.1 wt.% SiO_2 addition showed slight drop probably due to the inhomogeneous microstructure (see Fig. 3 (g)). Fracture strength of the sample with 0.5 wt.% SiO_2 addition was much improved to 28.2 MPa due to its homogeneous 3-D network structure. Fracture strength of the samples with ≥ 1.0 wt.% SiO_2 became smaller once again, due to the inhomogeneity of the microstructure as well as the

density drop (see Figs. 3 (i)-(k) and Fig. 2(b)).

4. Conclusions

We investigated the impurity effects on phase and microstructure stabilities of reactively-sintered porous MgTi_2O_5 . Appropriate Li_2CO_3 and SiO_2 doping promoted uniform grain growth with increased sintered density. However the coefficient of thermal expansion of Li_2CO_3 - and SiO_2 -doped MgTi_2O_5 ceramics decreased obviously above 900°C and 950°C due to the secondary sintering. To keep the fine-grained porous microstructure of Li_2CO_3 - and SiO_2 -doped samples with preventing the secondary sintering, impurity levels should be preferably limited less than ~ 1.0 wt.%.

Acknowledgements

A part of this work was supported by JSPS KAKENHI Grant Number JP16H04212 for Basic Research: Category B. We thank Dr. Kosuke Uoe and his colleagues at Sumitomo Chemical Co. Ltd. for kind measurements of the mercury porosimetry.

References

- [1] J. Adler, Ceramic diesel particulate filters, *Int. J. Appl. Ceram. Tech.* 2 (2005) 429-439
- [2] A. J. Pyzik, C. G. Li, New design of a ceramic filter for diesel emission control applications, *Int. J. Appl. Ceram. Tech.* 2 (2005) 440-451
- [3] C. K. Narula, C. Stuart Daw, J. W. Hoard, T. Hammer, Materials issues related to catalysts for treatment of diesel exhaust, *Int. J. Appl. Ceram. Tech.* 2 (2005) 452-466
- [4] K. Ohno, The SiC porous material technology which actualizes the development to diesel engine automobile business, (in Jpn.) *Ceram. Jpn.* 42 (2007) 431-438
- [5] S. B. Ogunwumi, P. D. Tepesch, T. Chapman, C. J. Warren, I. M. Melscoet-Chauvel, D. L. Tennent, Aluminum titanate compositions for diesel particulate filters, SAE Technical Paper 2005-01-0583, 2005.
- [6] I. J. Kim, Thermal stability of Al_2TiO_5 ceramics for new diesel particulate filter applications - a literature review, *J. Ceram. Proc. Res.* 10 (2009) 411-418
- [7] G. Bayer, Thermal expansion characteristics and stability of pseudobrookite-type compounds, Me_3O_5 , *J. Less-Common. Metal.* 24 (1971) 129-138
- [8] A. Nemoto, K. Iwasaki, O. Yamanishi, K. Tsuchimoto, K. Uoe, T. Toma, H. Yoshino, Development of innovative diesel particulate filters based on aluminum titanate: design and validation, R&D Report Sumitomo Kagaku, 2011-II (pp. 1-11)
- [9] E.A. Bush, F.A. Hummel, High-temperature mechanical properties of ceramic materials. 1. Magnesium dititanate, *J. Am. Ceram. Soc.* 41 (1958) 189-195

- [10] J.A. Kuszyk, R.C. Bradt, Influence of grain-size on effects of thermal-expansion anisotropy in MgTi_2O_5 , *J. Am. Ceram. Soc.* 56 (1973) 420-423
- [11] J.J. Cleveland, R.C. Bradt, Grain size/microcracking relations for pseudobrookite oxides, *J. Am. Ceram. Soc.* 61 (1978) 478-481
- [12] I. Shindo, Determination of the phase diagram by the slow cooling float zone method: the system MgO-TiO_2 , *J. Cryst. Growth* 50 (1980) 839-851.
- [13] J. Hauck, Crystallography and phase relations of $\text{MeO-M}_2\text{O}_3\text{-TiO}_2$ systems (Me=Fe, Mg, Ni; M=Al, Cr, Fe), *J. Solid State Chem.* 36 (1981) 52-65.
- [14] B.A. Wechsler, A. Navrotsky, Thermodynamics and structural chemistry of compounds in the system MgO-TiO_2 , *J. Solid State Chem.* 55 (1984) 165-180.
- [15] D. Taylor, Thermal expansion data: XI. Complex oxides, A_2BO_5 , and the garnets, *Br. Ceram. Trans. J.* 86 (1987) 1-6
- [16] B.A. Wechsler, R.B. von Dreele, Structure refinements of Mg_2TiO_4 , MgTiO_3 and MgTi_2O_5 by time-of-flight neutron powder diffraction, *Acta Cryst. B* 45 (1989) 542-549
- [17] Y. Suzuki, M. Morimoto, Porous $\text{MgTi}_2\text{O}_5/\text{MgTiO}_3$ composites with narrow pore-size distribution: in situ processing and pore structure analysis, *J. Ceram. Soc. Jpn.* 118 (2010) 819-822
- [18] Y. Suzuki, M. Morimoto, Uniformly porous MgTi_2O_5 with narrow pore-size distribution: in situ processing, microstructure and thermal expansion behavior, *J. Ceram. Soc. Jpn.* 118 (2010) 1212-1216
- [19] Y. Suzuki, Y. Shinoda, Magnesium dititanate (MgTi_2O_5) with pseudobrookite structure: a review, *Sci. Tech. Adv. Mater.* 12 (2011) no.034301
- [20] Y. Suzuki, T. S. Suzuki, Y. Shinoda, K. Yoshida, Uniformly porous MgTi_2O_5 with narrow pore-size distribution: XAFS study, improved in-situ synthesis, and new in-situ surface coating, *Adv. Eng. Mater.* 14 (2012) 1134-1138
- [21] Y. Nakagoshi, Y. Suzuki, Pseudobrookite-type MgTi_2O_5 water-purification filter with controlled particle morphology, *J. Asian Ceram. Soc.* 3 (2015) 334-338
- [22] Y. Nakagoshi, J. Sato, M. Morimoto, Y. Suzuki, Near-zero volume-shrinkage in reactive sintering of porous MgTi_2O_5 with pseudobrookite-type structure, *Ceram. Int.* 42 (2016) 9139-9144
- [23] H.-W. Son, R. S. S. Maki, B.-N. Kim, Y. Suzuki, High-strength pseudobrookite-type MgTi_2O_5 by spark plasma sintering, *J. Ceram. Soc. Jpn.* 124 (2016) 838-840
- [24] Y. Nakagoshi, Y. Suzuki, Dimensional change behavior of porous MgTi_2O_5 in reactive sintering, *Ceram. Int.* 43 (2017) 5541-5546
- [25] R.D. Shannon, Revised effective ionic radii and systematic studies of interatomic distances in halides and chalcogenides, *Acta Crystallogr. A* 32 (1976) 751-757

Table**Table 1** Content of raw materials and additives

Sample No.	MgCO ₃ (basic) (g)	TiO ₂ (anatase) (g)	Li ₂ CO ₃ (g)	Li ₂ CO ₃ (wt.%)
a	4.82	7.99	0	0
b	4.82	7.99	0.013	0.1
c	4.82	7.99	0.064	0.5
d	4.82	7.99	0.128	1.0
e	4.82	7.99	0.256	2.0
f	4.82	7.99	0.512	4.0

Sample No.	MgCO ₃ (basic) (g)	TiO ₂ (anatase) (g)	SiO ₂ (g)	SiO ₂ (wt.%)
g	4.82	7.99	0.013	0.1
h	4.82	7.99	0.064	0.5
i	4.82	7.99	0.128	1.0
j	4.82	7.99	0.256	2.0
k	4.82	7.99	0.512	4.0

Table 2 Total pore volume measured by the mercury porosimetry.

Samples	Pore volume (mL/g)
a (non doped)	0.49
c (Li ₂ CO ₃ -0.5)	0.33
e (Li ₂ CO ₃ -2.0)	0.30
h (SiO ₂ -0.5)	0.42
j (SiO ₂ -2.0)	0.26

Figure captions

- Fig. 1** XRD patterns of porous MgTi₂O₅ reactively sintered at 1100 °C with (a) Li₂CO₃ and (b) SiO₂ impurities.
- Fig. 2** Bulk density of porous MgTi₂O₅ with Li₂CO₃ and SiO₂ impurities. Relative density values (insert) were nominally calculated from the theoretical density of MgTi₂O₅, 3.644 g/cm³, without taking into account second phases. Volume shrinkage with Li₂CO₃ impurity is also demonstrated (insert): (a) non-doped porous MgTi₂O₅, (b)-(f) porous MgTi₂O₅ with Li₂CO₃ and (g)-(k) porous MgTi₂O₅ with SiO₂.
- Fig. 3** SEM micrographs of (a) non-doped porous MgTi₂O₅, (b)-(f) porous MgTi₂O₅ with Li₂CO₃ and (g)-(k) porous MgTi₂O₅ with SiO₂.
- Fig. 4** Pore-size distributions determined by mercury porosimetry.
- Fig. 5** Bulk thermal expansion of MgTi₂O₅ bars with various amount of Li₂CO₃ and SiO₂ impurities sintered at 1100 °C: (a,c) thermal expansion curves, and (b,d) linear thermal expansion.
- Fig. 6** Fracture strength of porous MgTi₂O₅ with Li₂CO₃ and SiO₂ impurities sintered at 1100 °C.

Figures

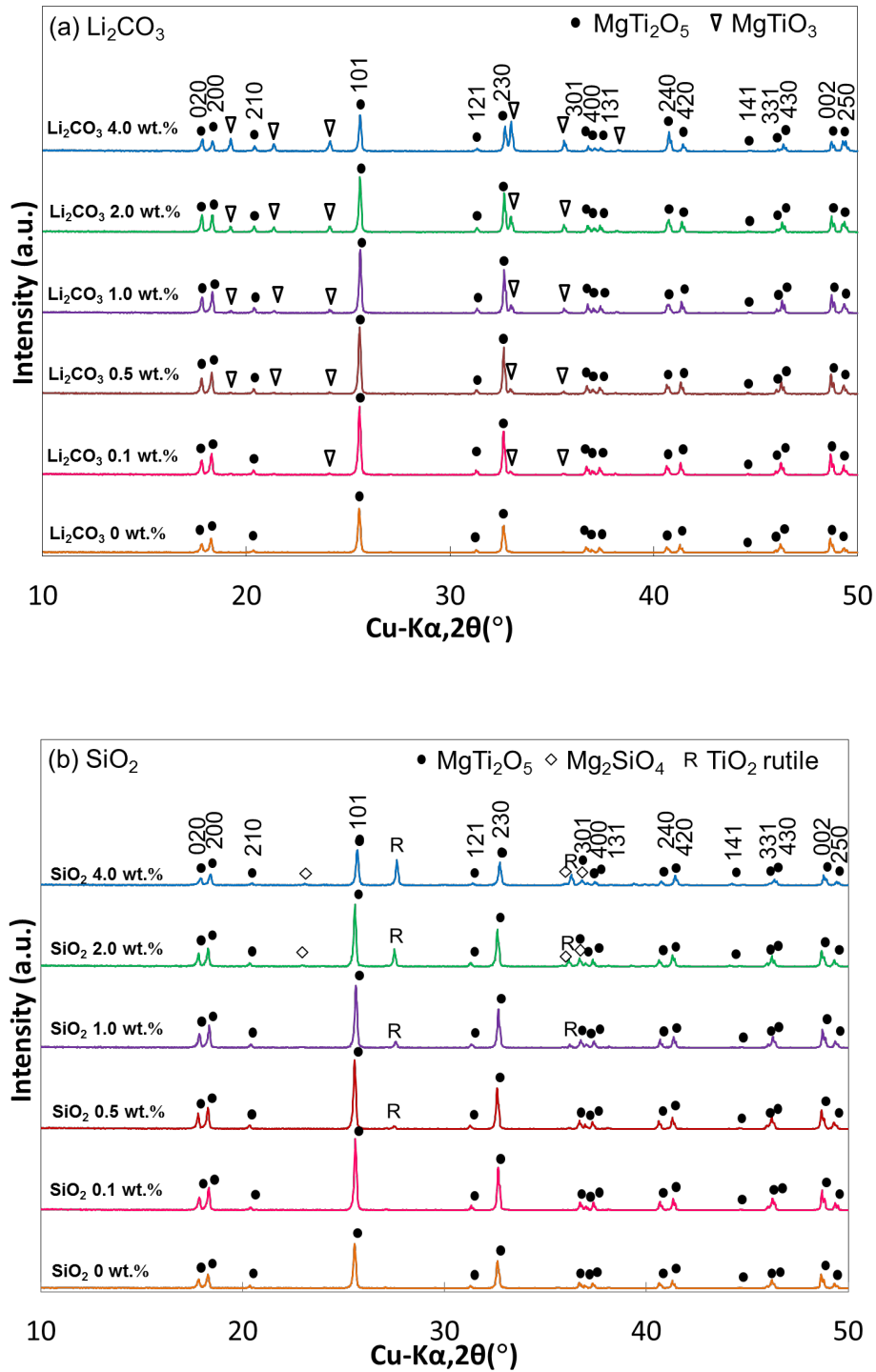


Fig. 1 XRD patterns of porous MgTi_2O_5 reactively sintered at $1100\text{ }^{\circ}\text{C}$ with (a) Li_2CO_3 and (b) SiO_2 impurities.

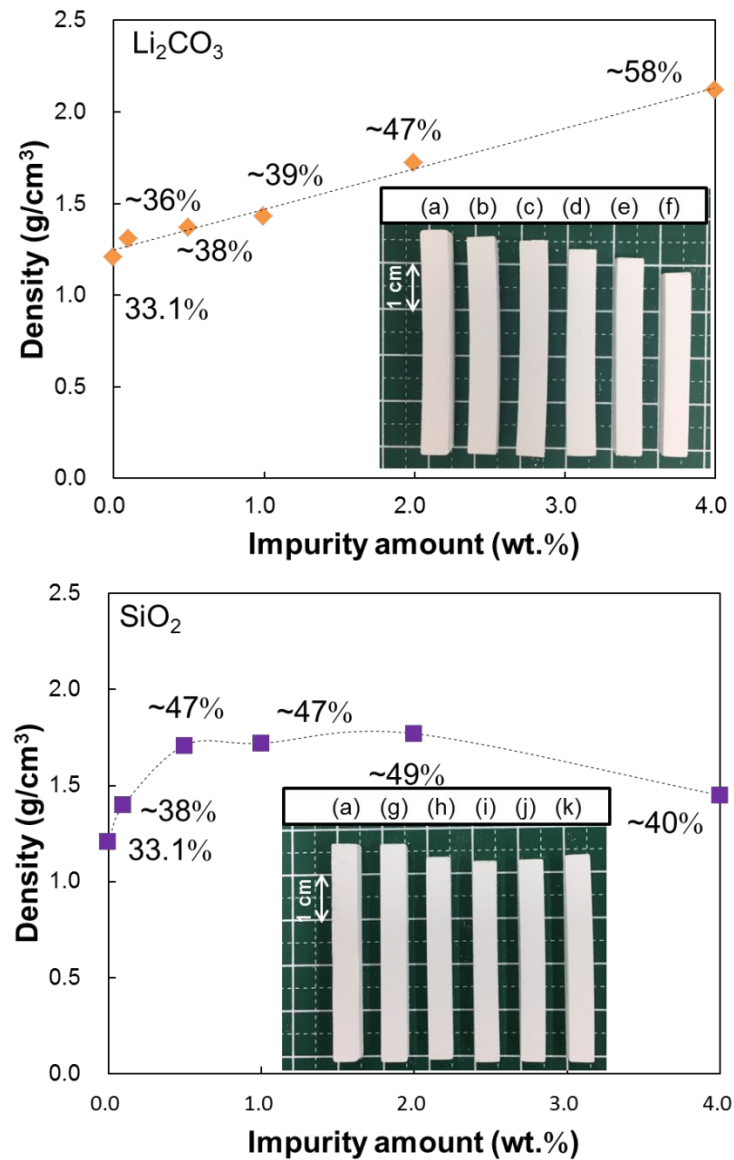


Fig. 2 Bulk density of porous MgTi₂O₅ with Li₂CO₃ and SiO₂ impurities. Relative density values (insert) were nominally calculated from the theoretical density of MgTi₂O₅, 3.644 g/cm³, without taking into account second phases. Volume shrinkage with Li₂CO₃ impurity is also demonstrated (insert): (a) non-doped porous MgTi₂O₅, (b)-(f) porous MgTi₂O₅ with Li₂CO₃ and (g)-(k) porous MgTi₂O₅ with SiO₂.

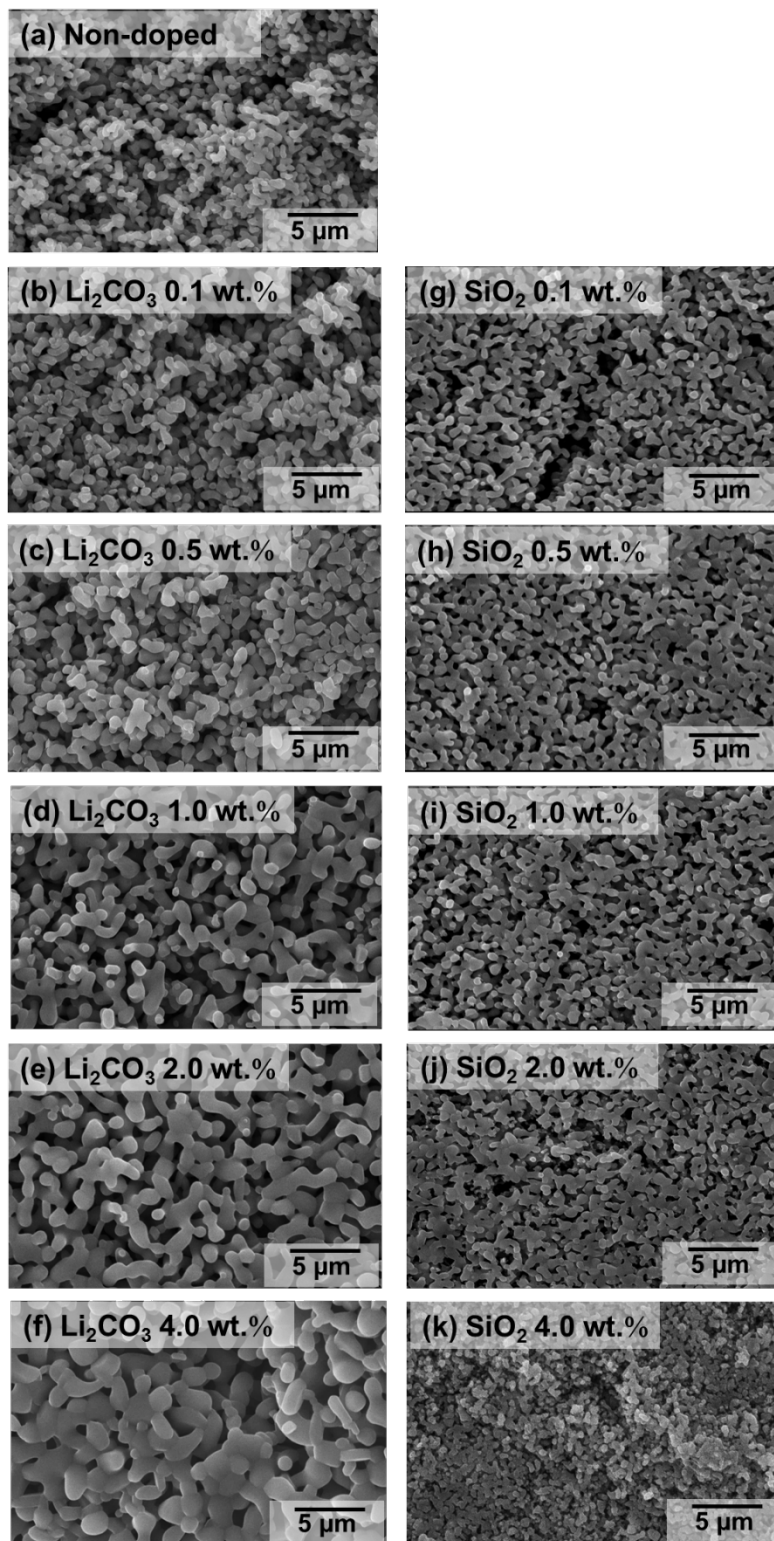


Fig. 3 SEM micrographs of (a) non-doped porous MgTi₂O₅, (b)-(f) porous MgTi₂O₅ with Li₂CO₃ and (g)-(k) porous MgTi₂O₅ with SiO₂.

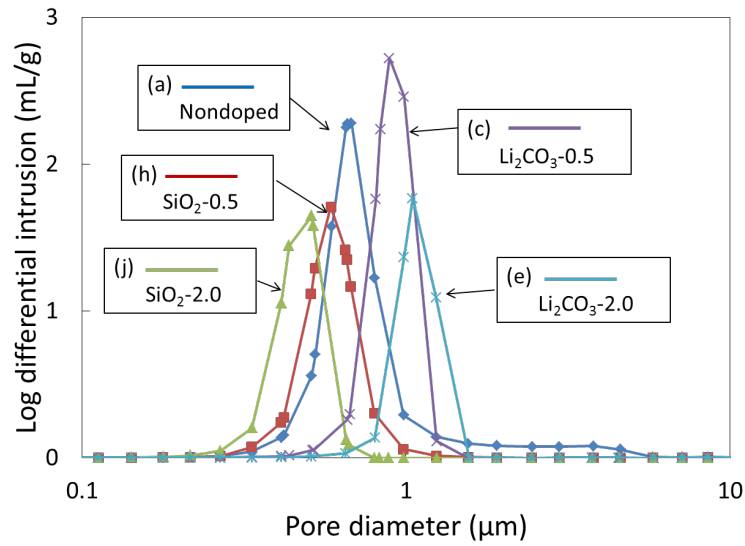


Fig. 4 Pore-size distributions determined by mercury porosimetry.

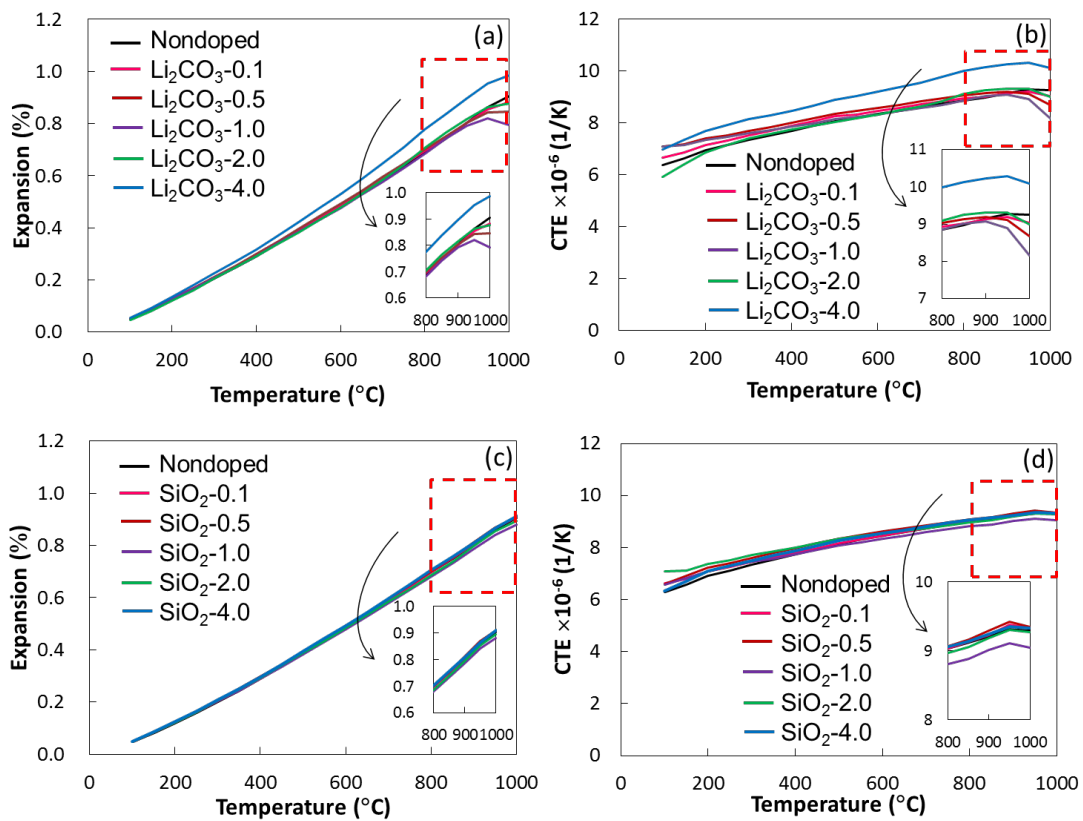


Fig. 5 Bulk thermal expansion of $MgTi_2O_5$ bars with various amount of Li_2CO_3 and SiO_2 impurities sintered at $1100\text{ }^\circ C$: (a,c) thermal expansion curves, and (b,d) linear thermal expansion.

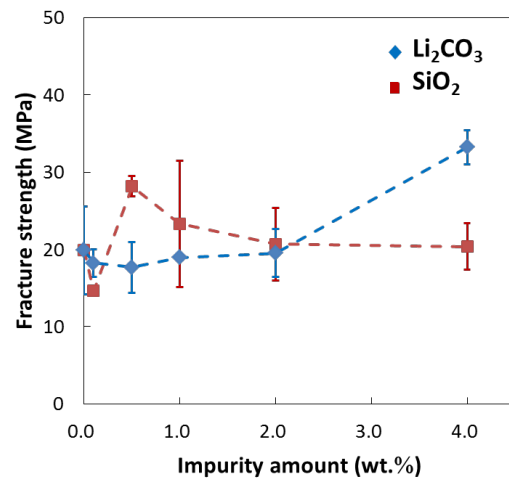


Fig. 6 Fracture strength of porous MgTi_2O_5 with Li_2CO_3 and SiO_2 impurities sintered at 1100 °C.